THE ASTROPHYSICAL JOURNAL, 468:871–882, 1996 September 10

A SEARCH FOR Fe III IN SN 1006 USING THE HOPKINS ULTRAVIOLET TELESCOPE

WILLIAM P. BLAIR
Department of Physics and Astronomy, Johns Hopkins University, Charles and 34th Streets, Baltimore, MD 21218; wpb@pha.jhu.edu
KNOX S. LONG
Space Telescope Science Institute, 3700 San Martin Drive, Baltimore, MD 21218; long@stsci.edu
AND
JOHN C. RAYMOND[1]
Harvard-Smithsonian Center for Astrophysics, 60 Garden Street, Cambridge, MA 02138; jraymond@cfa.harvard.edu
Received 1996 January 16; accepted 1996 March 20

ABSTRACT

We have observed the 912–1840 Å spectrum of the sdOB star known as the Schweizer-Middleditch star, which lies behind the remnant of SN 1006, to search for absorption lines due to the unshocked ejecta. We have also observed the sdB star PG 0839+399 for comparison. The spectra were obtained using the Hopkins Ultraviolet Telescope on the Astro-2 Space Shuttle mission in 1995 March. Assuming SN 1006 was a Type Ia supernova, 0.3–0.5 $M_\odot$ of iron should be present in the expanding remnant. The X-ray spectrum shows no evidence for this quantity of iron in the hot gas, indicating that this material may still be interior to the reverse shock. Broad absorption lines of Fe II have been seen in the spectrum of the Schweizer-Middleditch (SM) star previously but can only account for a small fraction of the expected iron. Our spectrum covers the region of the strongest expected Fe III resonance line at 1123 Å. We use stellar model fits to the spectra to constrain the strength of Fe III and Fe II lines in the spectral region below Lyα. Absorption from Fe III is inferred in our spectrum of the SM star, but at a nominal level of only 1.0 Å equivalent width, below the value of $\sim$2.3 Å predicted with the current best model provided by Hamilton & Fesen. However, the Hamilton & Fesen model is not precluded by the statistics in our data, which provide a 3 σ upper limit of 3.4 Å for the equivalent width of Fe III λ1123. Converting into mass, our best fit corresponds to only 0.016 $M_\odot$ of Fe^{++}, and the 3 σ limit corresponds to $\leq$0.054 $M_\odot$ of Fe^{++}. This indicates that if the expected iron is present in the ejecta, it must be largely in ionization states higher than Fe^{++}. No other absorption lines attributable to the supernova remnant are detected in the spectrum below Lyα. A faint excess in the spectrum near 1170 Å is unexplained but might be due to Lyα emission from the nonradiative shock on the near side of the supernova remnant shell. This possibility is testable with improved optical data for SN 1006.

Subject headings: shock waves — supernovae: individual (SN 1006) — supernova remnants — ultraviolet: ISM

1. INTRODUCTION

SN 1006 provides a unique opportunity to study a young supernova remnant (SNR) of a Type Ia explosion (Minkowski 1966; Schaefer 1996). Not only is its age known precisely, but its distance is also known from proper motion studies and spectral velocity measurements of a faint filament of pure Balmer line emission that stretches across the northwest sector of the remnant (van den Bergh 1976; Schweizer & Lasker 1978; Kirshner, Winkler, & Chevalier 1987; Long, Blair, & van den Bergh 1988; Smith et al. 1991; Raymond, Blair, & Long 1995). In particular, using improved models of fast, nonradiative shocks, Laming et al. (1996) have constrained the shock velocity at the position of the optical filament to be 2600 ± 300 km s^{-1}. With a proper motion of this same filament of $0''.30 \pm 0''.04$ per year (Long et al. 1988), the distance is 1.80 ± 0.3 kpc. While other more indirect methods have suggested distances mostly in the 1.5–2 kpc range (see Schaeffer 1996, Table 7 and references therein), this result reduced the error bars on the kinematically allowed distance considerably. We will assume this revised distance throughout this paper.

Because of the relatively high Galactic latitude of SN 1006 ($\sim 14^\circ.6$; Green 1995), the line of sight to the remnant is relatively free of extinction. X-ray and radio observations show a nearly circular, strongly limb-brightened shell structure with angular diameter $\sim 30'$ (Pye et al. 1981; Reynolds & Gilmore 1986; Winkler & Long 1996). With our revised distance, this corresponds to a diameter of 15.8 pc, implying a mean expansion rate of $\sim$7600 km s^{-1}. Koyama et al. (1995) and Willingale et al. (1996) have reported spatially resolved *ASCA* and *ROSAT* X-ray data that show thermal emission throughout the remnant, although the bright X-ray rims are dominated by the power-law spectrum seen in previous X-ray spectra (Becker et al. 1980b; Leahy, Nousek, & Hamilton 1991, and references therein). The absence of thermal emission had been considered puzzling since other young, shell-like SNRs are dominated by thermal processes (see Becker et al. 1980a, 1980c).

The other fortuitous circumstance that makes SN 1006 unique is the presence of a UV-bright background star seen in projection just $\sim 2'$ from the center of SN 1006. This star, which we will refer to as the "SM star," was discovered by Schweizer & Middleditch (1980, hereafter SM80), and was suspected originally to be the stellar remnant of the explosion. However, Savedoff & Van Horn (1982) demonstrated convincingly that the star is behind the SNR. Thus, the SM star provides a means of probing the interior of the remnant by looking for absorption lines due to the cold SNR ejecta

[1] Astro-2 Guest Investigator.

(Wu et al. 1983). The SM star is faint visually, but very blue (see Table 1). Weak optical He II lines compared with the hydrogen Balmer lines point to an sdOB spectral type (see Simon, Hunger, & Kudritzki 1981). SM80 estimated the distance to be $1.1^{+1.4}_{-0.6}$ kpc; our distance estimate points toward the upper end of the allowed range. SM80 also derived $E(B-V) = 0.112 \pm 0.024$, consistent with measurements of the continuum dip near 2200 Å (Fesen et al. 1988). The rising spectrum to shorter wavelengths is largely responsible for the utility of this relatively faint star in searching for absorption from the SNR.

The near-UV spectrum of the SM star was first investigated with the *International Ultraviolet Explorer* (*IUE*) satellite by Wu et al. (1983). This spectrum showed a blue stellar continuum and evidence for broad absorption lines near 2380 and 2600 Å due to Fe II. Higher signal-to-noise data obtained subsequently with *IUE* (Fesen et al. 1988) and more recently with the *Hubble Space Telescope* (*HST*) and the Faint Object Spectrograph (FOS) (Wu et al. 1993) have confirmed this early measurement. The Fe II absorption lines have equivalent widths of $W_\lambda \sim 15$ Å and Doppler widths of FWHM ~ 8000 km s^{-1}, indicating the presence of rapidly expanding, cold iron within the interior of the remnant. This is particularly interesting since the well-developed theory of Type Ia supernovae, i.e., the deflagration of a carbon-oxygen white dwarf (Nomoto, Thielemann, & Yokoi 1984; Garcia-Senz & Woosley 1995, and references therein), demands 0.3–0.5 $M_\odot$ of iron in the expanding ejecta. However, Hamilton & Fesen (1988) performed a careful analysis of the Fe II absorption profiles and concluded that only 0.014 $M_\odot$ of iron can be in the form of Fe II, only 4%–5% of the amount expected from the best-fitting Type Ia model. Hamilton & Fesen (1988) accounted for this by assuming the majority of the iron is ionized to Fe III and higher by the X-ray/EUV emission from the reverse shock, with 2.6 times as much Fe^{++} predicted for the best-fitting model. The strongest expected resonance line of Fe III is located at 1123 Å, too short in wavelength for observation with *HST* or *IUE*.

In this paper we describe a search for Fe III absorption in the spectrum of the SM star, carried out with the Hopkins Ultraviolet Telescope (HUT) during the Astro-2 Space Shuttle mission, which launched on 1995 March 2 UT for a 16 day flight on *Endeavour* (STS-67). Section 2 describes the observations and data reductions for both the SM star and a comparison sdB star with similar characteristics. Section 3 discusses stellar model fitting to the data for both stars. We then summarize the atomic parameters for the iron (and other) transitions of interest to the SM star discussion in § 4. In § 5 we place constraints on the presence of Fe III λ1123 in the spectrum of the SM star, and discuss other implications of our data. Section 6 provides a summary of our results.

2. OBSERVATIONS AND REDUCTIONS

A technical description of the HUT instrument is given by Davidsen et al. (1992). HUT employs an f/2 0.9 m primary mirror and a prime focus Rowland spectrograph with a microchannel plate–intensified photon-counting detector. Spectral coverage spans the 820–1840 Å spectral range with 2048 0.51 Å bins. The resolution for a point source is 3 ± 1 Å, depending on pointing quality and wavelength. New silicon carbide optical coatings on the primary mirror and on the spectrograph grating improved the sensitivity by a factor of 2.3 for Astro-2, with a peak effective area of 24 cm^2 near 1100 Å. Further details of the instrumental performance and calibration during Astro-2 are discussed by Kruk et al. (1995).

Far-ultraviolet spectra of the SM star were obtained with HUT during two separate pointings on Astro-2, on 1995 March 6 and 9. Both observations were carried out with a 12″ circular aperture. This choice of aperture was made to minimize airglow contamination in the faint target, at the risk of a loss of photometric accuracy. Despite its faintness, the SM star was visible in the HUT acquisition camera and the Shuttle crew was able to place the object in the aperture manually for both observations.

During an observation, HUT's internal computer reports the positions of the centroided guide stars, permitting the

TABLE 1

OPTICALLY DERIVED STELLAR PARAMETERS

Parameter	SM Star	Reference	PG 0839+399	Reference
$T_{\rm eff}$(K)	38500 ± 4500	1	36100 ± 500	2
	~43000	3	~40300	3
log g	6.7 ± 0.6	1	5.91	2
	~6.0	3	~6.0	3
V or y	16.74 ± 0.02 (V)	1	14.39 ± 0.05 (y)	4
$B-V$ (observed).....	− 0.14 ± 0.02	1	− 0.29	5
$E(B-V)$	0.112 ± 0.024	1	0.00 ± 0.02	2
	0.10 ± 0.02	6	~0.045	3
	~0.12	3		
M_v	6.2 ± 1.8	1	...	
Distance (kpc)	1.1(+1.4, − 0.6)	1	...	
	1.5–3.3	7		
	≥1.8	8		

REFERENCES.—(1) Schweizer & Middleditch 1980; (2) Saffer et al. 1994; (3) this paper; see discussion and Table 2; (4) Wesemael et al. 1992; (5) derived from Wesemael et al. 1992, using formula of Green 1980; (6) Wu et al. 1993; (7) Fesen et al. 1988; (8) kinematic distance to SN 1006; Laming et al. 1996.

pointing stability to be assessed. During the first observation, the pointing drifted by $\pm 4''$ with occasional spikes to higher values. Analysis of the count rate and pointing errors showed correlated changes with time. By the time of the second observation, the pointing and telescope focus were improved. The pointing stability for the second observation was excellent ($<1''$ rms) and the count rate was stable, but at a value roughly 75% of the peak count rate in the first observation. Although this is due partly to a small loss in sensitivity of the instrument between the two observations (see Kruk et al. 1995), the primary cause is most likely light loss from the aperture due to miscentering of the target. This can happen if a minor pointing disturbance occurs during the setup for the observation (between placing the object in the aperture and locking onto the guide stars). With a point spread function of 4.5″ FWHM (Kruk et al. 1995), observations in the 12″ aperture are particularly susceptible to this effect. As mentioned above, we are less concerned with the absolute photometry of the star than we are with the spectral shape, and so no corrections have been applied to the fluxes derived below.

Each observation began roughly halfway through orbital night and proceeded through the night-into-day terminator until the target approached the 20° bright earth limb constraint. The HUT detector was read out in "histogram" mode, which produces a histogram of the data every 2 s. Each observation occurred in the following way: The detector was turned on during the acquisition phase to measure the airglow background at the start of each observation. After the target was acquired and observed for an initial period, the payload specialist manually moved the HUT pointing position $\sim 1'$ to a "sky" position for 5 minutes, and then returned to the target position. Another sky observation was performed for the last several minutes of each pointing, which was well into the daylit portion of the orbit. These airglow observations suffice to show the kinds of variations occurring in the airglow lines, which are sensitive to a wide variety of parameters, but are not of sufficient quality that they can be scaled and subtracted from the target data per se. In each case, the first and second sky observations show little sky contamination beyond Lyα and perhaps very faint O I λ1304, but numerous fainter lines are apparent in the third (daylit) sky spectra of each pointing.

The object data were extracted and summed for each of the two pointings separately. Furthermore, we separately extracted the portion of each observation that was judged to have little or no obvious airglow contamination beyond Lyα. This was done by setting "windows" around airglow features in the spectrum and plotting the count rates as a function of time for each observation. Observation I contained 1784 s of data (416 s free of airglow), while observation II contained 1338 s of integration (634 s free of airglow). Each of these counts spectra was converted to a flux scale using a special HUT package developed within IRAF and the calibration described by Kruk et al. (1995), based on model atmosphere fits to spectra of DA white dwarfs observed during the mission. The uncertainties in wavelength are less than 0.2 Å and those in the relative intensity calibration are less than 5%. Since the sensitivity of HUT varied during Astro-2, we have interpolated calibration curves that are appropriate for each observation and applied these individually to the observations. The separate pointings were then averaged, weighting by exposure times, to produce combined spectra representing the 1050 s low-airglow data and the entire 3122 s integration on the target. (Since HUT is a photon-counting instrument, the tasks in the HUT package permit the proper treatment of error arrays that are carried along with the spectra during processing.) The top panel of Figure 1 shows the total flux–calibrated spectrum for the SM star, both as observed and after applying an extinction correction of $E(B-V) = 0.11$, using the extinction curve formulation of Cardelli, Clayton, & Mathis (1989) with $R_v = 3.1$. For comparison, the flux level at 1600 Å is $\sim 20\%$ below the value observed with the FOS by Wu et al. (1993), consistent with the above discussion of the nonphotometric properties of the HUT data for this observation. While the "low-airglow" spectrum is considerably noisier than the total spectrum, this spectrum will be used in the next section to provide a more accurate assessment of the Lyβ, Lyγ, and Lyδ absorption-line depths in the stellar spectrum.

We also observed an sdB star with characteristics similar to the SM star to provide a comparison of stellar spectral features; this is particularly important given that no appropriate comparison spectra exist for the spectral region below 1200 Å. We selected a star from the PG catalog (Green, Schmidt, & Liebert 1986) that had been studied by Saffer et al. (1994). This star, PG 0839+399 (or PG 0839 for short), is considerably brighter and less reddened than the SM star (see Table 1), but has a similar temperature and surface gravity. It was observed with HUT on 1995 March 8 with a total usable integration of 866 s, mostly in orbital night. Except for Lyα emission and a region at 1304 Å where the cumulative effects of O I airglow bombardment have caused a decreased sensitivity in the HUT detector, this spectrum is unaffected by airglow contamination at any significant level. This spectrum was processed in a manner similar to the description above. The observed, flux-calibrated spectrum of PG 0839 is shown in the bottom panel of Figure 1.

Comparison of these two spectra shows several similarities and one obvious difference. Both objects display fairly blue spectra with emission all the way down to the Lyman limit at 912 Å. Lyman absorption lines are present in both objects (see Lyδ at 952 Å), although Lyβ and to some extent Lyγ in the SM star are contaminated by airglow emissions. Other lines seen in hot, solar abundance stellar atmosphere models (including C IV $\lambda\lambda$1548, 1551, C III λ1176, Si IV $\lambda\lambda$1393, 1402, and He II λ1085) are weak or absent in the spectra of both objects, indicative of below solar abundances in the atmospheres of both stars. The obvious difference is the strong absorption feature at 1283 Å in the spectrum of the SM star, seen previously with *IUE* (Fesen et al. 1988) and attributed to possible Si II or S II absorption λ1260 redshifted by ~ 6000 km s^{-1}, or O I λ1304 blueshifted by about the same amount; no corresponding feature is seen in PG 0839. Possible weak, broad depressions near 1330 and 1420 Å correspond to the features in the *IUE* data reported by Fesen et al. (1988). We see no clear evidence of the *IUE* feature reported near 1608 Å and attributed to Fe II, although the noise level in our spectrum at these wavelengths may preclude detection. However, we do see evidence for a broad feature centered near 1550 Å that may have been marginally detected with *IUE*.

In the region below 1200 Å, a very weak, broad depression may be present in the region near 1130 Å, but no obvious absorption due to the expected Fe III feature is present. In addition, there appears to be structure in the

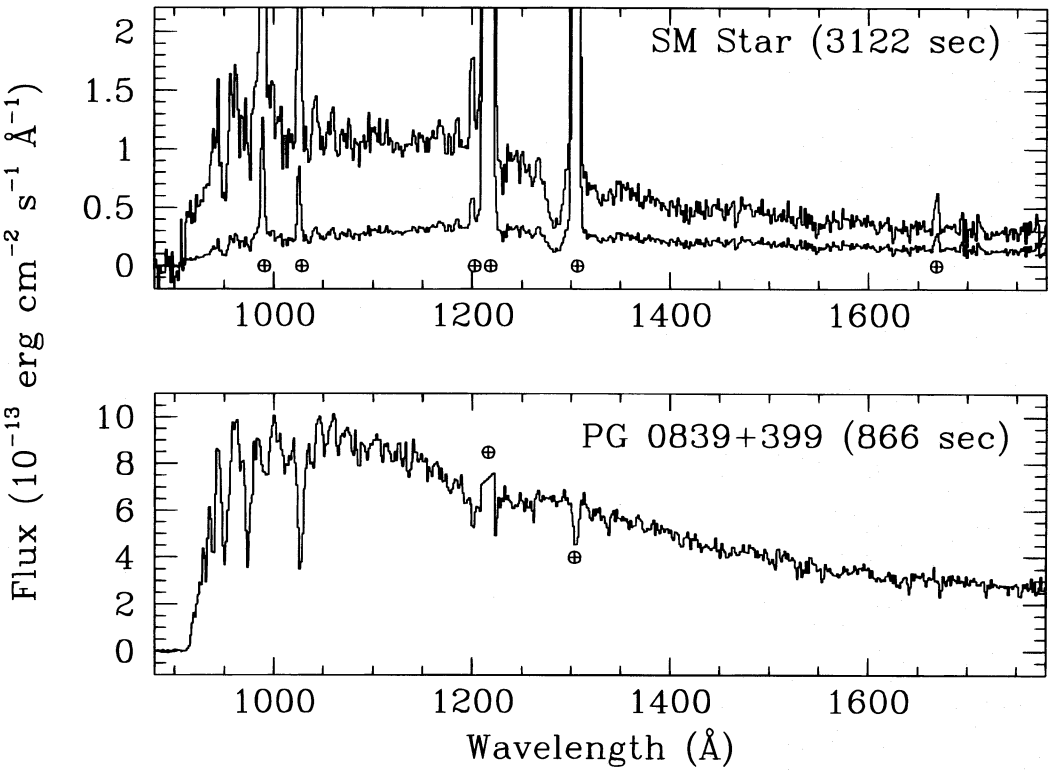

FIG. 1.—Flux-calibrated HUT FUV spectra of the SM star (*top panel*) and the sdB star PG 0839+399 (*bottom panel*), obtained during the Astro-2 mission in 1995 March. The SM star spectrum is shown as observed (*bottom curve*) and after correction for $E(B-V) = 0.11$ assuming a standard extinction curve (see text). Emission lines, marked with an Earth symbol, are all due to residual airglow. The dip near 1283 Å in the SM star is due to absorption from the SNR, while the dip at 1304 Å in PG 0839 is a detector flaw caused by the cumulative effects of strong O I airglow bombardment at this location on the detector. These data have been binned by three pixels for use in this figure.

spectrum below ~1100 Å above the noise level. The reality of these features will be examined further below.

3. STELLAR MODEL FITTING

The properties of both PG 0839 and the SM star have been derived from optical observations of the stars, which are summarized in Table 1. Much of the information listed for the SM star derives from the discovery paper (SM80) and the photometry described therein, while the information on PG 0839 derives from Saffer et al. (1994) and Wesemael et al. (1992). In an effort to better constrain the characteristics of the SM star, we have borrowed the original tracings of the high-resolution photographic spectra discussed in SM80 from Francois Schweizer and digitized them; Rex Saffer (1996, private communication) attempted to fit the digitized data using the techniques described in Saffer et al. (1994) but was unable to improve on the data listed in Table 1 with this data set. A good optical spectrum with a modern detector is needed to reduce the errors on the parameters for the SM star.

We have calculated a grid of stellar models for use in fitting the spectra of PG 0839 and the SM star. The fits to PG 0839 will provide a "control" of how well the models do in describing a normal subdwarf star, and the fits to the SM star will provide an expectation against which we can judge the presence of broad absorptions due to the SNR. The model spectra were constructed using the pair of programs TLUSTY and SYNSPEC (Hubeny, Lanz, & Jeffrey 1994; Hubeny & Lanz 1995; Lanz & Hubeny 1995). We ran test cases varying log g and assumed abundances before deciding on a model grid. The stellar parameters of the two stars are similar but not exactly the same, and abundances in subdwarfs are distinctly nonsolar and variable from star to star (see Saffer & Liebert 1994). To keep the problem tractable, however, we have chosen not to vary abundances individually. Models with metals set at 0.01 solar abundance approximately reproduced the stellar C III λ1176 and C IV $\lambda\lambda$1548, 1551, and we have fixed the abundances at this level. The model grid was then generated with log g values of 6.0 and 7.0 and a temperature range from 25,000 to 45,000 K in 1000 K increments. Only hydrogen and helium opacities were used in TLUSTY for determining the pressure, temperature, and density as a function of depth in the atmosphere. (The assumption of just H and He instead of solar abundances in TLUSTY has very little effect on the structure calculation in this temperature range.) We then used this structure to calculate spectra assuming 0.01 solar abundances for the atmosphere. The spectra were calculated on a very fine grid ($\Delta\lambda \leq 0.015$ Å), convolved with a Gaussian (FWHM = 3.5 Å) to approximate the HUT resolution, and then resampled to match the HUT bin size.

With this grid in hand, we have applied a nonlinear χ^2 minimization routine called SPECFIT within the HUT package in IRAF (see Kriss 1994) to perform a number of model fits to these data. SPECFIT uses various model inputs and assumptions set by the user and adjusts parameters, constrained by the error array for the data. The program can read in a specified grid of stellar models and interpolate to find the best-fitting temperature. Likewise, a grid of H_2 absorption models can be provided to assess

whether the pattern of lines expected from H_2 absorption below 1108 Å is present. The H_2 models, described in detail by Bowers et al. (1995), were calculated for $T = 80$ K, Doppler parameter $b = 10$ km s^{-1}, and log $N(H_2) =$ 15–20. These parameters are representative of values expected from interstellar absorption but should not be construed as an accurate fit to the H_2 along these lines of sight (which would require much higher resolution data). Interstellar extinction, assuming the curve of Cardelli et al. (1989), can be taken into account within the fitting and either fixed or allowed to vary. Finally, other model components, including Gaussian absorption and/or emission lines, can be added as desired.

We first performed fits of PG 0839. The log $g = 6.0$ model grid provided much better fits to the Lyman line widths than the log $g = 7.0$ grid (in keeping with the optical determination of log $g = 5.91$), and closer approximations to the optically determined temperature. However, we find that the HUT spectrum can be matched better by adding some interstellar reddening. Table 2 lists a summary of model fits, showing a significantly improved fit for PG 0839 when the reddening parameter was allowed to vary. The reddening and temperature both affect the overall continuum shape, however, and the model with reddening has a higher temperature than that determined optically. We note the presence of narrow interstellar absorption lines in the HUT spectrum of PG 0839 at 1200, 1260, 1526 Å, etc., which are consistent with interstellar material along this line of sight. We also see a pattern of weak dips in the spectrum shortward of ~1100 Å that are not matched by the stellar models. As shown in Table 2, the addition of H_2 absorption lowers the χ^2 statistic considerably, with a best-fit column of $N(H_2) = 1.8 \times 10^{17}$ cm^{-2}, again consistent with some interstellar absorption toward PG 0839. Figure 2 shows the best-fit model for PG 0839 with $E(B-V) = 0.045$ (including H_2 absorption). The stellar model fits to PG 0839 are encouraging, with good agreement in the overall spectral shape and depth of the Lyman lines. Most of the power in the remaining χ^2 distribution is attributable to the narrow regions between the lower Lyman lines, where our assumption of 3.5 Å resolution provides a relatively poor match to the actual resolution (which is closer to 2.5 Å at these wavelengths; see Kruk et al. 1995). We note particularly the reasonable fit in the 1100–1200 Å spectral region, where no strong stellar features appear to be present. We move on now with a degree of confidence to fitting the SM star spectrum.

For the SM star, we first fitted the 1050 s data section that was extracted to be least affected by airglow contamination. This data set is lower in signal-to-noise ratio because the SM star is some 30 times fainter than PG 0839, so we have binned the HUT data over four pixels. The Lyman series is present and should be relatively free of airglow, at least in the case of Lyγ and Lyδ, providing an important "goodness of fit" criterion. We have included a broad absorption due to the obvious SNR line near 1283 Å in the fitting procedure, but at this stage ignored other lines that may be present. Initial experiments with both log $g = 6.0$ and log $g = 7.0$ models and with various abundance sets again showed a superior fit with log $g = 6.0$ and 0.01 solar abundance scaling. This log g value is at the lower end of the range allowed by the optical data (see Table 1), but the Lyman lines in the log $g = 7.0$ models are definitely too broad (even though the HUT data have been binned). The log $g = 6.0$ grid will be assumed in the discussion below.

As summarized in Table 2, we fit this spectrum assuming the optically determined values of T and $E(B-V)$, and then allowed these parameters to vary; only regions around the core of Lyα and the O I 1304 Å airglow features have been removed from the fit. As with PG 0839, better fits were achieved with higher temperatures and somewhat higher reddening, although the changes needed are smaller than for PG 0839. Figure 3 shows this spectrum with the nominal and "best-fit" models overlaid for comparison. The small changes in reddening and temperature allow the overall slope of the spectrum to be better matched. While Lyγ and Lyδ are fit reasonably by these models, Lyβ appears to be filled in, indicating that some weak airglow contamination is present at Lyβ even in this extraction of the data. The bottom line from these fits is that models using parameters close to those expected from the optical analysis of the SM star provide reasonable fits to the HUT spectrum.

The total SM star data set provides a somewhat improved signal-to-noise ratio, but we choose to bin over three pixels to ensure good statistics. This spectrum shows indications of other broad lines from the SNR (as seen with *IUE*) in the region longward of Lyα. These include features

TABLE 2

SUMMARY OF SPECTRAL FITS[a]

Object	Ranges (Å)	T/σ (K)	$E(B-V)/\sigma$	χ^2/dof	χ^2_r	Comments
PG 0839	923–1207, 1225–1300, 1310–1840	36100	0.00	10546/1700	6.20	Using fixed optical parameters
PG 0839	923–1207, 1225–1300, 1310–1840	40180/400	0.051/0.015	2908/1702	1.71	Includes strong IS lines
PG 0839	923–1207, 1225–1300, 1310–1840	40300/350	0.045/0.005	2618/1706	1.53	Includes $N(H_2) = 1.8 \times 10^{17}$ cm^{-2}
SM star no airglow section	923–1207, 1225–1300, 1310–1840	38500	0.11	539/426	1.27	Using fixed optical parameters; bin 4 data; includes 1283 SNR line
SM star no airglow section	923–1207, 1225–1300, 1310–1840	39650/1700	0.136/0.007	491/427	1.15	Bin 4 data; includes 1283 SNR line; Lyβ not well fit
SM star total	[b]	38500	0.11	791/527	1.50	Broad components at 1283, 1330, 1420, and 1550; bin 3 data
SM star total	[b]	43500/1400	0.138/0.005	675/532	1.27	Same as above
SM star total	[b]	42900/1200	0.119/0.005	557/530	1.05	Includes $N(H_2) = 10^{18}$ cm^{-2} and all predicted broad absorptions from Table 3

[a] All stellar models log $g = 6.0$ and 0.01 solar abundances. Where shown, 1 σ statistical errors were determined from a grid of fits and a $\Delta\chi^2$ contour for two free parameters, corrected for χ^2_r. The possibility of systematic errors means that these errors are only lower limits to the real uncertainties.

[b] To avoid airglow lines, SM star total fits used regions as follows: 923–983, 993–1020, 1029–1195, 1227–1296, 1313–1662, 1672–1840 Å.

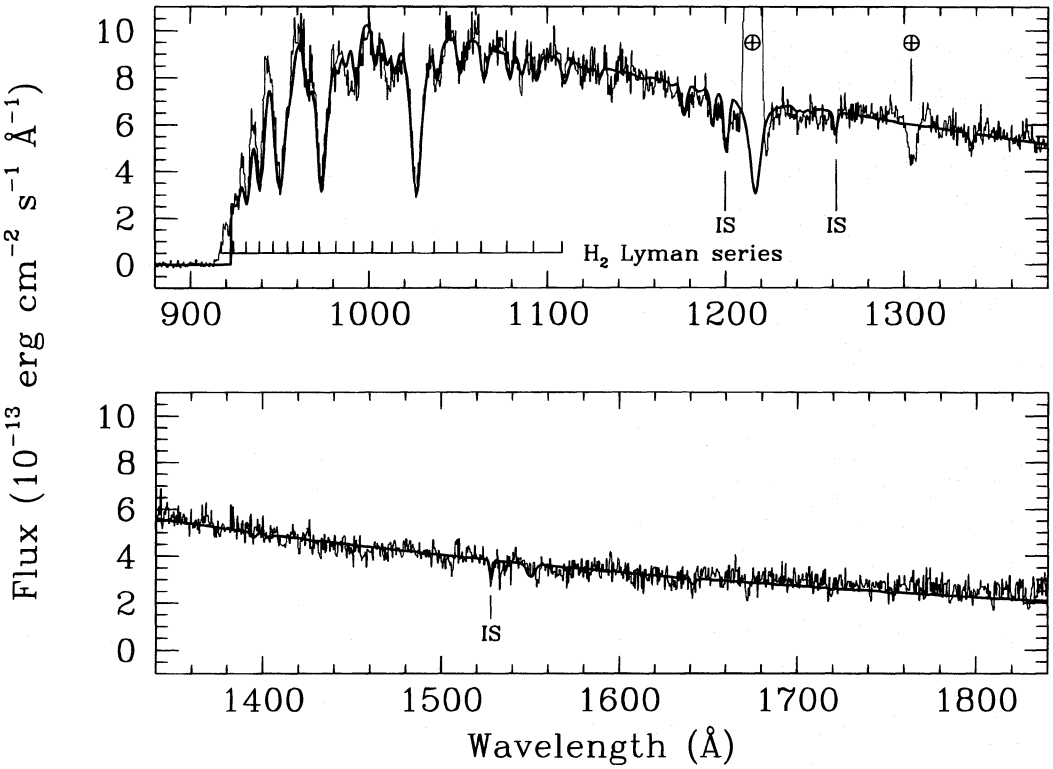

FIG. 2.—Reduced HUT spectrum of PG 0839+399 is shown by the histogram, with the best-fitting model from Table 2 superposed as a smooth line. Several strong interstellar absorption lines are indicated. Strong Lyman absorption lines of hydrogen are clearly visible (Lyα is masked by airglow) and the presence of H_2 absorption is indicated below 1108 Å. (Only the H_2 Lyman bands are shown for simplicity, although Werner bands are also present.)

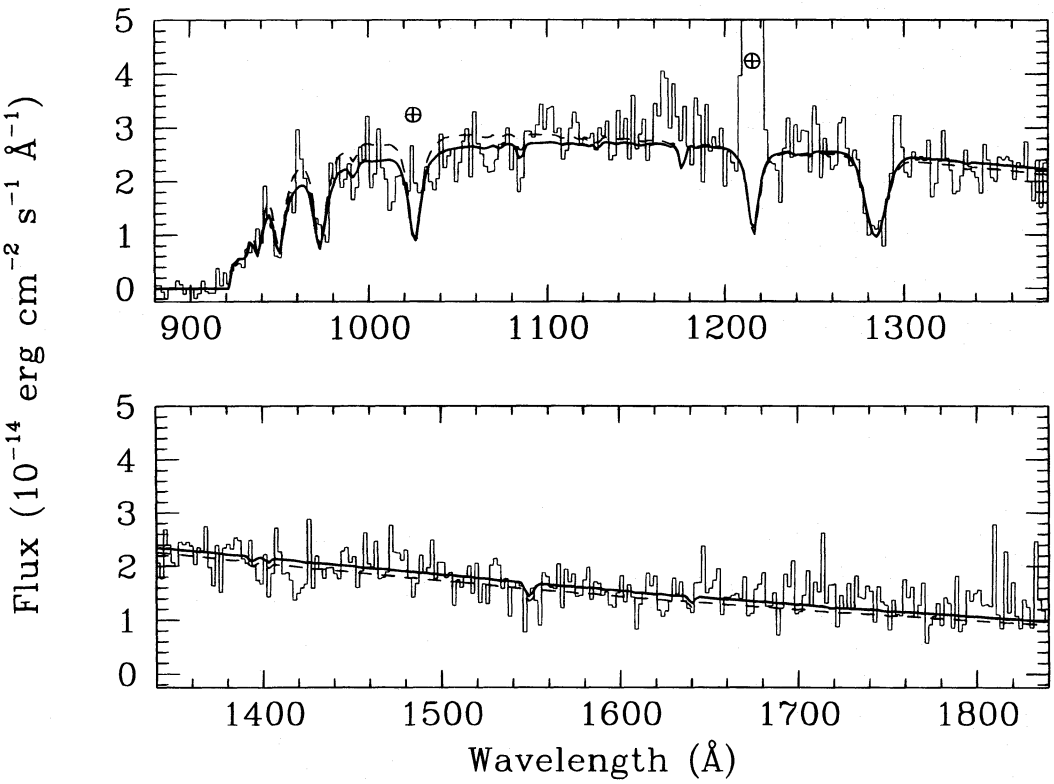

FIG. 3.—1050 s "no airglow" section of SM star data is shown as the histogram, after binning over four pixels (~2 Å). The solid curve shows the best-fitting model from Table 2, while the dashed curve shows the model with T and $E(B-V)$ fixed at their optically determined values. Note that Lyβ is partially filled in by airglow emission, but Lyγ and Lyδ are matched reasonably well.

near 1330 and 1420 Å, and 1550 Å, in addition to the 1283 Å feature. (The identification of these features will be discussed in the next section.) We have added broad Gaussian components in SPECFIT to account for each of these features, letting the program determine the best-fitting centroids and widths of the lines. We fit this spectrum cutting out only those regions around the known airglow lines in the spectrum, as summarized in Table 2. Again, improvement is seen when the fixed temperature and $E(B-V)$ are allowed to vary, and the sense of the change is the same as with PG 0839. The higher temperature in the best-fitting model may partially reflect the fact that weak airglow emissions fill in both Lyβ and Lyγ in the total data set, making the absorption lines appear weaker; the large σ on the temperature reflects the uncertainty in this number. With the improved signal-to-noise ratio of this data set, the distinctive pattern of H_2 absorption again becomes apparent below 1108 Å. Adding the H_2 model grid in to SPECFIT improves the χ^2 of our fits dramatically, as seen in Table 2. The best-fit model has $N(H_2) = 10^{18}$ cm^{-2}, somewhat higher than for PG 0839, in keeping with the higher $E(B-V)$ for the SM star. Figure 4 shows this best-fitting model superposed on the total SM star data set.

The only portion of this spectrum not well fitted by the model is a small excess of flux in the 1160–1190 Å region. This excess is present in each observation individually, and is visible in the "low-airglow" data sections of each observation as well (albeit at lower statistical significance). The fit to PG 0839 (and to numerous white dwarf calibration stars) is good through this region, which excludes a significant calibration error. From inspection of other HUT data, there are no faint airglow lines that could blend together to account for the observed excess. We have also used separate HUT observations of the Lyα airglow line to model the shape of the scattering wings from this strong line, scaling the derived profile to match the Lyα flux actually determined from the airglow portions of the SM star observations. This scaled profile is included in the fit shown in Figure 4. The Lyα scattering wings are far too weak to explain the observed excess. Finally, we have been unable to conceive of a realistic model involving an elevated stellar continuum that fits the $\sim$1170 Å flux but is absorbed by SNR absorptions at other (shorter and longer) wavelengths. Hence, we are left with the impression that the excess is real, but with no obvious instrumental explanation.

An intriguing possibility, given the already unusual spectrum of this star, would be broad, blueshifted Lyα emission from the nonradiative shock wave on the near side of the SNR shell. However, if the excess is fitted with a single, broad, blueshifted Gaussian, it is centered near 1178 Å ($\Delta v = -9500 \pm 4000$ km s^{-1}) and requires an uncomfortably large FWHM $= 9000 \pm 2700$ km s^{-1}. The total flux required, $2.5 \pm 0.6 \times 10^{-13}$ ergs cm^{-2} s^{-1} Å^{-1} through the 12″ aperture, corresponds to a surface brightness of $2.2 \pm 0.5 \times 10^{-15}$ ergs cm^{-2} s^{-1} arcsec^{-2}, or about 72 ± 17 R. (We note that an excess about half this size could be tolerated in the 1240–1270 Å region, depending on the stellar model used in the fitting.) While the velocities required are substantial, the uncertainties are large and the surface brightness is not entirely out of the question. A broad Lyβ component was observed with HUT in the northwest optical filament (Raymond et al. 1995) with a flux

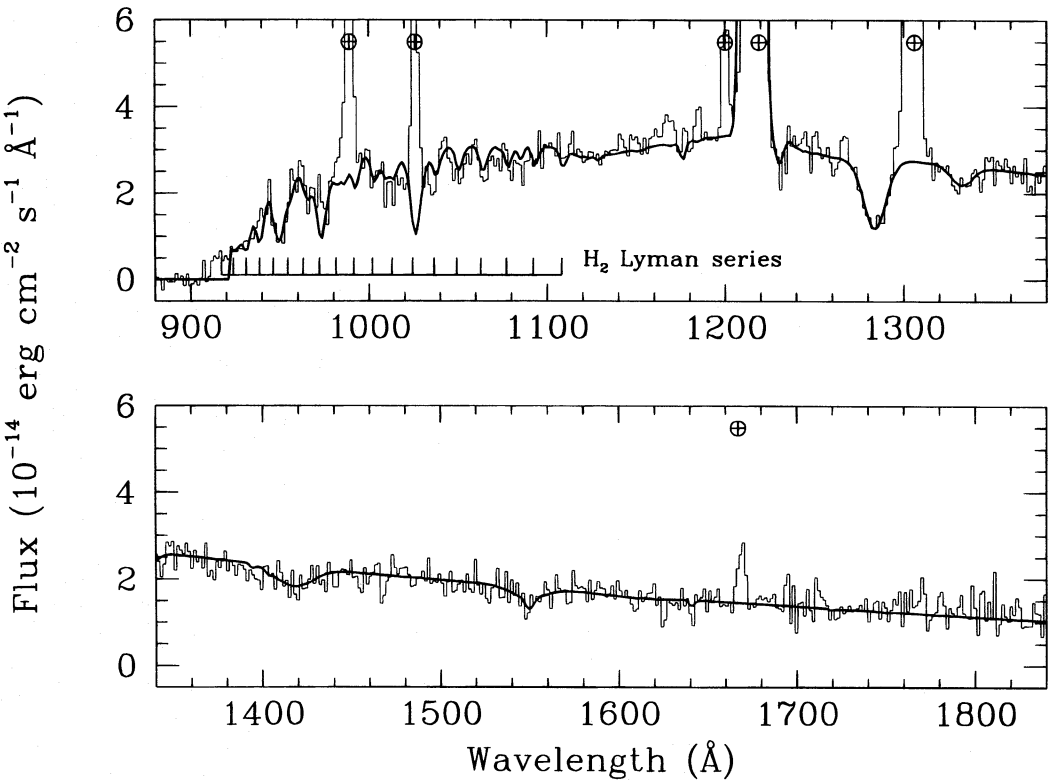

FIG. 4.—SM star "total" data set, binned over 3 pixels ($\sim$1.5 Å), is shown as the histogram. The solid curve is the best-fitting model from Table 2, including H_2 absorption. Broad components have been fitted to SNR absorption lines as shown in Table 3. This fit includes a Lyα emission profile, derived from separate airglow spectra observed by HUT and scaled to the observed Lyα flux in the airglow spectra obtained during the SM star observations. Note that the excess flux in the 1160–1190 Å region cannot be explained by wings of this Lyα profile.

near 5.6×10^{-13} ergs cm^{-2} s^{-1} Å^{-1}. Assuming this flux arises from roughly one-fourth of the HUT 19″ × 196″ aperture (for this edge-on filament), and assuming a ratio of Lyα:Lyβ ~ 6 (appropriate for a fast shock), the predicted Lyα flux through the 12″ aperture used for the SM star observation would be $\sim 4 \times 10^{-13}$ ergs cm^{-2} s^{-1} Å^{-1}.

A direct consequence of this interpretation would be the expectation of a comparable feature seen in Hα. It is not clear that existing observations can rule out this possibility, but neither do they provide confirmation. Current optical spectra of the SM star (SM80) do not extend to the red region necessary to test this prediction, although no evidence for such a feature associated with Hβ is present. Narrowband Hα CCD imaging has been performed for SN 1006 (Winkler & Long 1996), and these data do not support the presence of diffuse Hα emission near the observed position, although the limit is only at a level of less than 30% of the surface brightness of the northwest optical filament. The broad component of Hα associated with the purported Lyα feature would be shifted out of the bandpass of these narrowband images, but the nonradiative shock theory predicts a narrow component near rest velocity that might be expected to be detectable in these images. This possibility can be tested conclusively with new optical data. For now, we leave the fit to this excess emission out of our overall model for the SM star spectrum until the reality of this component can be confirmed. However, the presence of this excess emission in the spectrum of the SM star complicates our ability to measure the presence of any broad Fe III λ1123 absorption, which would be adjacent at shorter wavelengths.

4. ABSORPTION-LINE FITTING

We start this section by summarizing what is known about the broad absorptions due to SN 1006 in the spectrum of the SM star. The most obvious features are the broad absorptions near 2380 and 2600 Å attributed to strong Fe II resonance transitions centered near rest wavelength (Wu et al. 1993), and the strong absorption line near 1283 Å, with weaker absorptions near 1330, 1420, and 1550 Å (Fesen et al. 1988). The most recent and highest quality fits to the Fe II lines are by Wu et al. (1993) using the FOS. They derive a deconvolved line profile for a single line having FWHM = 8000 km s^{-1} centered near the rest wavelength; although the line profile is not strictly Gaussian, it is fairly symmetric. With the quality of our data, we make the simplifying assumption of Gaussian line profiles with this FWHM for fitting other Fe lines in the HUT wavelength range. As described above, we have already assumed Gaussian absorption profiles for the other proposed SNR absorption lines, but we let the centroids and FWHMs be fit by the SPECFIT program. Table 3 summarizes the fits to these features from the HUT data.

Fesen et al. (1988) provide a good discussion of the possible line identifications for these broad absorption lines. To us the simplest and most consistent interpretation is that they are *all* due to silicon lines *redshifted* by 5000–6000 km s^{-1}, in some cases blended with significant rest wavelength narrow interstellar or stellar absorptions. Inspection of line lists such as Table 3 of Morton, York, & Jenkins (1988) shows that Si IV λλ1393, 1402 is the only reasonable identification for the feature near 1420 Å, implying a redshift near 5000 km s^{-1} for the centroid and accounting for the relatively broad appearance of this line. Of the various possibilities for the 1283 Å feature (cf. Fesen et al. 1988), Si II λ1260 becomes the obvious choice (although other lines could be blended with it). If mainly due to Si II, this feature is shifted by ~5400 km s^{-1} and has a FWHM = 3400 km s^{-1}. The much weaker depressions near 1330 and 1550 Å can then be attributed to Si II lines from 1304 and 1526 Å, respectively, at the appropriate redshift and similar line widths. Alternate identifications (e.g., C IV at rest for the 1550 Å feature, or shifted O I λ1304 for the 1283 and/or 1330 Å features) can be disregarded because of the absence of other lines of the same element that should be present but are not seen. We note in passing that Koyama et al. (1995) concluded that Si is at least an order of magnitude overabundant in their *ASCA* spectra of the thermal X-ray component in SN 1006, while other elements such as O and Ne appear closer to solar abundance.

The reality of these features is confirmed, and the identifications are strengthened, by inspection of archival *HST* FOS G130H data, which not only shows these broad lines, but also shows a broad, red wing on the stellar Lyα absorption line that is attributable to redshifted Si III λ1206. (Overplotting the HUT and FOS data shows that the downward dip in the HUT data just redward of the geocoronal Lyα line is actually the onset of this absorption.) We note in passing the absence of any strong Si I lines that might be present (rest wavelengths 1255, 1562, and 1631 Å) as well as the absence of Fe I resonance lines at longer wavelengths (see Hamilton & Fesen 1988; Wu et al. 1993). Hence, at the moment the only known SNR lines can be attributed to very broad (~8000 km s^{-1}) Fe II near rest wavelength and broad (~3500 km s^{-1}) lines of Si II, Si III, and Si IV redshifted by ~5500 km s^{-1}.

Given these facts, we can predict the strengths of other lines that might be present in the region below Lyα, assuming the lines of interest are unsaturated. The absorption produced by the various SNR lines will depend on the column density of each ion present, its velocity spread, the oscillator strengths of the transitions involved, and their relative wavelengths. In the case of an actual observed equivalent width (W_λ), predictions for other lines of an ion can be made (or for other ions if the relative column densities are known). In Table 3, we show a compilation of oscillator strengths for the strongest Fe II and Fe III ground-state–connected resonance lines in the near- and far-UV, including the Fe II lines whose W_λ's have been observed (Fesen et al. 1988; Wu et al. 1993). References are given for the atomic data used. The observed W_λ's are shown in parentheses. We show the predicted W_λ's for these lines (numbers without parentheses) using the strongest Fe II line at 2382 Å for scaling, viz.,

$$W(\lambda) = f(\lambda)/f(2382)(\lambda/2382)^2 W(2382) ,$$

where λ is the wavelength in Å. The prediction for Fe III λ1123 assumes that there are 2.6 times as many Fe III atoms as Fe II, which is the prediction of the best-fitting model described by Hamilton & Fesen (1988). Inspection of Table 3 shows that most of the far-UV iron transitions are expected to be very weak, with only Fe II λ1145 and Fe III λ1123 expected above 1 Å equivalent width. These two lines should blend together and are likely responsible for the weak, broad dip near 1130 Å visible in the SM star spectrum, as seen in Figure 1.

Table 3 also contains information for Si lines expected in the far-UV. Predictions for Si II lines are based on the

TABLE 3

OSCILLATOR STRENGTHS AND EQUIVALENT WIDTHS[a]

Ion/λ (Å)	f-value	Reference	W_λ (Å)	Comments
			Iron Lines[b]	
Fe II 2599.4	0.2239	1	(14.8)	Wu et al. 1993 FOS measurement
	0.224	2	13.7	Predicted
2586.7.....	0.0646	1, 2	3.9	Predicted
2587+2599	...	...	(15.2 ± 1.0)	Fesen et al. 1988 *IUE* measurement
2382.0.....	0.300	1	(15.4)	Wu et al. 1993 FOS measurement
	0.301	2		
2373.7.....	0.0282	1, 2	1.4	Predicted
2374+2382	...	...	(19.0 ± 1.0)	Fesen et al. 1988 *IUE* measurement
2343.5.....	0.110	1, 2	5.5	Predicted
	...	...	(9.4 ± 2.0)	Fesen et al. 1988 *IUE* measurement
Fe II 1608.5	0.0619	1, 2	1.4	Predicted
	...	...	(4.3 ± 1.0)	Fesen et al. 1988 *IUE* measurement
	...	...	(<2.5)	Wu et al. 1993 FOS limit
Fe II 1260.5	0.025	2	0.36	Predicted
Fe II 1144.9	0.105	1, 2, 3	1.2	Predicted, strongest of three lines
	0.133	4	1.6	Predicted with this f-value
Fe II 1122.0	0.020	1, 2	0.35	Predicted, sum of two lines
1125.4.....	0.011			
Fe II 1096.9	0.032	1, 2	0.34	Predicted
1082.0.....	0.018	1	0.19	Predicted
	0.014	2	0.15	Predicted with this f-value
1063.2.....	0.0645	1	0.66	Predicted
	0.0600	2	0.61	Predicted with this f-value
Fe II 940.2.....	0.0121	1, 2	0.10	Predicted
937.7	0.0195	1, 2	0.15	Predicted
926.2	0.0438	1, 2	0.34	Predicted
Fe III 1122.5.....	0.0788	1	2.3	Predicted values assuming 2.6 times as much Fe III as Fe II, and f-values indicated
	0.068	5	2.0	
	0.0537	6	1.6	
	0.0797	2	2.4	
	...	...	(1.0)	Best fit, this paper
	...	...	(<3.4)	3 σ upper limit, this paper
			Silicon Lines[c]	
Si II 1260.4	0.96, 1.18	2, 7	...	Used below
(1281)	...	...	(7.9 ± 0.6)	Fesen et al. 1988 measurement
(1283.9/0.6)	...	...	(9.0 ± 0.8)	This paper; $V = 5600$ km s^{-1}
Si II 1190.4	0.2502	1	...	Shifted into Lyα
1193.3.....	0.4991	1	...	Shifted into Lyα
Si II 989.7	0.133	1	0.62–0.77	Predicted at 1005 Å
1020.7.....	0.028	1	0.14–0.17	Predicted at 1038 Å
Si II 1304.4	0.087–0.147	2, 7	0.71–1.5	Predicted based on HUT W_λ(1260)
(1331)	...	...	(1.8 ± 0.3)	Fesen et al. 1988 measurement
(1332.4/2.5)	...	...	(2.5 ± 0.9)	This paper; $V = 6400$ km s^{-1}
Si II 1526.7	0.13–0.23	2, 7	1.5–3.2	Predicted based on HUT W_λ(1260)
(1549.1/4.9)	...	...	(3.4 ± 1.3)	This paper; $V = 4400$ km s^{-1}
Si III 1206.5	1.669	1	...	Shifted into Lyα
Si IV 1393.8	0.524	2	...	
1402.8.....	0.260	2	...	
(1420)	...	...	(3.7 ± 0.4)	Fesen et al. 1988 measurement
(1418.6/3.8)	...	...	(5.0 ± 1.7)	This paper; $V = 4700$ km s^{-1}

[a] Numbers in parentheses are measured values; numbers without parentheses are predictions.

[b] For Fe II, predictions based on scaling from Wu et al. 1993 measurements of strongest line at 2382 Å, using relative f-values and ratio of wavelengths squared.

[c] For Si II, predictions based on observed strength of 1283 Å dip, assuming it is due entirely to Si II λ1260, using relative f-values and ratio of wavelengths squared.

REFERENCES.—(1) Morton 1991; (2) Verner, Barthel, & Tytler 1994; (3) Shull, van Steenberg, & Seab 1983; (4) Nahar 1995; (5) Fawcett 1989; (6) Ekberg 1993; (7) Shull, Snow, & York 1981.

observed W_λ of the 1283 Å feature, assuming it is entirely due to Si II λ1260. In general, there is more variation in the published f-values for these transitions, and the predicted W_λ's of the Si II lines in Table 3 show the full range given these uncertainties. Given that the strongest expected line in the region below Lyα produces an expected W_λ of less than 1 Å, it is unlikely that Si lines contribute significantly in the sub-Lyα region.

To test whether the combined effects of the numerous weak absorption lines in the sub-Lyα region are significant, we have added Gaussian absorptions at the W_λ's predicted in Table 3, fixing the Fe line widths at FWHM = 8000 km

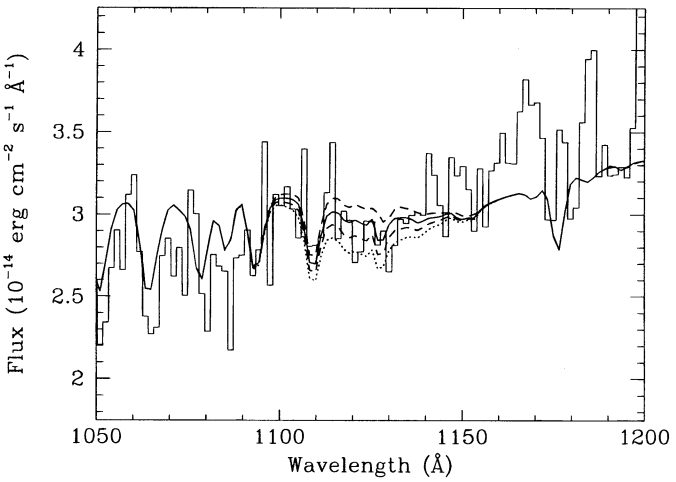

FIG. 5.—Enlargement of the region around the position of Fe III λ1123, showing the SM star total spectrum (*histogram*) and various model assumptions for the Fe III line. The solid curve shows the best fit, which has a broad Fe III line with 1.0 Å equivalent width. The top dashed line assumes no Fe III line is present, while the bottom dashed line assumes W(1123) = 2.0 Å. The dotted line is for W(1123) = 3.0 Å. None of these curves are excluded at the 3 σ level from the best fit (see Table 4).

s^{-1} and fixing the Si lines at FWHM = 3500 km s^{-1}. (In reality, these lines were already incorporated into the SM star "total" data set fits listed in Table 2.) The inclusion of these extra lines made very little difference in the shape of the sub-Lyα continuum (and hence the best-fit parameters), and only the strongest three lines (Si II λ989 at 1005 Å, Fe II λ1145, and Fe III λ1123) had an observable effect.

What can we say about Fe III absorption in the spectrum of the SM star? The final fit listed in Table 2 and shown in Figure 4 includes an assumed Fe III absorption at W(1123) = 2.3 Å (assuming Morton's 1991 *f*-value) with a width the same as observed for Fe II at longer wavelengths, as well as Fe II λ1145 with W(1145) = 1.6 Å and the same width. We have applied SPECFIT using the global fit derived above, but changing the assumptions locally for the Fe III line to judge the presence of this feature in the spectrum.

In Figure 5, we show the 1050–1200 Å region of the SM star total spectrum, with the data in histogram format. Overlaid as smooth lines are various SPECFIT outputs showing different assumptions about the strength of the assumed Fe III absorption line. The solid curve shows the best fit when the equivalent width is free to be varied, which has W(1123) = 1.0 Å. The dashed lines above and below the solid line show the fit assuming 0.0 and 2.0 Å equivalent width for the Fe III line, respectively, while the dotted line shows a 3.0 Å assumption. In Table 4, we compile statistics on these and other models as determined from SPECFIT. These tests show that some Fe III absorption is likely to be present, but at a level below that predicted by Hamilton & Fesen (1988). As shown by the probability column in Table 4, there is only a 10% chance that the Fe III absorption is as strong as predicted by the Hamilton & Fesen (1988) model. However, using $\Delta\chi^2$ to determine the standard deviation (see Press et al. 1986), only equivalent widths above 3.4 Å are excluded at the 3 σ level, indicating that the model proposed by Hamilton & Fesen (1988) is allowed within the statistics.

TABLE 4

SUMMARY OF Fe III FITS IN SM STAR

W(1123)	$\Delta\chi^2$	Probability	σ
0.0	1.3	0.25	1.1
1.0[a]	0.0	...	...
2.0	1.6	0.20	1.3
2.3	2.7	0.10	1.6
3.0	6.2	0.01	2.5
3.4	9.0	0.0027	3.0
4.0	13.7	< 0.001	3.7

[a] The model with W(1123) = 1.0 Å provided the smallest χ^2 value (571.33 for 541 dof) when W was allowed to vary; χ^2_r = 1.056. Other models are referenced to this one.

5. DISCUSSION

Hamilton & Fesen (1988, hereafter HF88) discuss a detailed model for SN 1006 to account for the various observed properties of the remnant. Their model attributes the X-ray emission in SN 1006 to thermal emission, dominated by the reverse shock, in a state of extreme nonionization equilibrium and into the outer layers of ejecta where the composition is distinctly nonsolar (see. Hamilton, Sarazin, & Szymkowiak 1986). The cold, inner layers of ejecta, including the predicted iron, are interior to the reverse shock (assumed to be near 5000 km s^{-1} in velocity space) and are being ionized by the X-ray/EUV emission from the reverse shock. HF88 use two different models for the deflagrated white dwarf star and find a superior fit assuming a model by Woosley & Weaver (1987). Using this model, they calculate the relative ionization fractions of Fe I–V as a function of time, predicting 2.6 times as many Fe^{++} ions as Fe^{+}. As shown in Table 3, depending on the assumed *f*-value and scaling from the strong Fe II lines in the near-UV, the predicted Fe III λ1123 line from this model would have an equivalent width near 2 Å.

Taking our best fit at face value indicates that there may be less Fe III than predicted by the best-fitting model of HF88. This may be more compatible with expectations, given that the HF88 discussion was based on assumptions about the X-ray spectrum that are now known to be incorrect. While Koyama et al. (1995) have demonstrated conclusively for the first time that a fraction of the X-ray emission is indeed thermal, this component is relatively faint and distributed fairly uniformly over the face of the SNR (as opposed to the limb-brightened shell that might be expected from a reverse shock origin). The dominant component of the X-ray emission is apparently synchrotron emission concentrated on the northeastern and southwestern rims of the remnant. This will influence the estimate of the density of the ambient medium, and thereby affect the computation of the luminosity in the EUV, which in turn determines the predicted ionization state of the unshocked iron interior to the reverse shock. Likewise, the realization that the Fe II line profile extends out to ~8000 km s^{-1} in velocity space (Wu et al. 1993), instead of the 5000 km s^{-1} assumed by HF88, points to a weaker reverse shock, and thus less ionization of the cold ejecta than assumed by HF88. Given that Wu et al. (1993) estimate the mass fraction of Fe II to be only 0.014 $M_\odot$ out to 8000 km s^{-1}, less ionization (and consequently weaker Fe III) is in the wrong direction to account for the missing iron expected from SN 1006, assuming a Type Ia SN picture. Assuming the same model

for conversion of column density into mass, our best fit corresponds to only 0.016 $M_\odot$ of Fe^{++}, and our 3 σ limit corresponds to ≤ 0.054 $M_\odot$ of Fe^{++}. Hence, the HUT observation does not alleviate the problem of the "missing iron" in SN 1006, indicating a substantial fraction of the iron ejecta, if present, must be at still higher ionization stages.

The good fits to the HUT spectra using the stellar models described above and a standard interstellar extinction curve have other implicit ramifications. The stellar models fit fairly well, indicating that there is no large-scale missing opacity in the models or other fundamental problem. The fit to the PG 0839 UV spectrum demands a significant level of interstellar extinction that is not inferred from the optical data, but the character of this extinction is well modeled with the standard curve. The fact that the SM star spectrum is also well matched using the standard extinction curve, along with the presence of both narrow interstellar lines and H_2 absorption, implies that most of the extinction toward the SM star really is *interstellar*; evidently, we can look directly through ~ 0.4 $M_\odot$ of Fe and other ejecta without there being a substantial effect on the extinction curve, assuming the Fe is really there. We have no direct information on grain formation or the grain size distribution that might be expected in the ejecta of a Type Ia supernova; if the grains were large compared to 1000 Å, one could hide arbitrarily large amounts and not affect the far-UV extinction curve, although then infrared emission would be expected from that portion of the dust that had encountered the reverse shock, and this is not observed (Dwek et al. 1987).

Are broad SNR lines of any elements besides Fe and Si present in the spectrum of the SM star? The fact that the features observed are so broad and the star is so faint makes it difficult to answer this question with certainty. There are no glaring differences between our model and the data shown in Figure 4, although some differences below 1100 Å are not precluded. The *ASCA* X-ray data are consistent with sulfur and possibly magnesium being overabundant along with silicon (Koyama et al. 1995). There are no strong Mg resonance lines expected in our wavelength range, and there is no evidence of Mg II λ2800 absorption (at rest or redshifted) in the FOS data of Wu et al. (1993). It might be possible to hide potential lines of sulfur, especially if they arise at or near the redshift and FWHM of the Si lines discussed earlier. The strongest ground-state–connected lines of S II are several lines close to the Lyman limit at 912 Å that would be shifted up to ~ 925 Å (not obviously present or required by our data) and the lines at 1250.6, 1253.8, and 1259.5 Å that could be blended with the Si II feature at 1283 Å. The strongest expected S III lines are at 1190.2 Å (which would be shifted into Lyα) and 1012.5 Å (which would be shifted into Lyβ). Finally, given the presence of Si IV, the S IV line at 1062.7 Å might be expected near 1081 Å under these assumptions. The presence of this latter line at a low level is not excluded by our data, although the uncertainty in the H_2 absorption-line strengths in this region make it difficult to set a meaningful limit.

6. SUMMARY

The HUT far-UV spectra of both the sdB star PG 0839+399 and the SM star can be well fitted using the current generation of non-LTE stellar atmosphere models. It is interesting, however, that in both cases the HUT spectra seem to require more interstellar extinction and a higher effective temperature than predicted from the optical photometry of these stars. A systematic error in the HUT calibration at the $\leq 5\%$ level cannot be ruled out and may be partially responsible for these differences, but the overall continuum shape is not the only parameter used in fitting the models to the data. In the case of PG 0839+399, the presence of narrow interstellar and H_2 absorption lines are incompatible with the optical determination of $E(B-V) = 0.0$, showing that at least part of the observed effect is real.

In the portion of the SM star spectrum longward of Lyα, we confirm the presence of several broad absorption lines due to the supernova remnant and suggest that they arise from transitions of Si II, Si III, and Si IV redshifted by ~ 5500 km s^{-1}. Below Lyα, only Fe II λ1145 and Fe III λ1123 are predicted to be at an observable level, and the presence of both are inferred from our model fits to the data. The nominal best fit shows Fe III λ1123 to be weaker than expected by a factor of 2.3, but the best predicted value is allowed within the statistics. Our upper limit of ≤ 0.054 $M_\odot$ on the mass of Fe^{++} indicates either that much of the expected 0.3–0.5 $M_\odot$ of iron in the expanding ejecta is in higher ionization stages, or it is simply not present at the expected level. A low level excess in the spectrum between 1160 and 1190 Å may be due to broad, blueshifted Lyα emission from the nonradiative shock front on the near side of the expanding remnant. No other SNR absorptions in the spectral region below Lyα have been identified in our data.

It will be important to obtain a high-quality optical spectrum of the SM star to permit the uncertainties in the optically determined characteristics of the star to be reduced. This will permit a more accurate model to be calculated and used in fitting the UV spectral region covered by the HUT data. In addition, such a spectrum could be searched for evidence of a broad, blueshifted Hα component that should be present if the 1170 Å excess in the HUT data is due to Lyα from the SNR shell. A better knowledge of the H_2 absorption along this line of sight would permit a higher fidelity fit to this component and would permit better limits to be placed on other potential absorption lines in the far-UV. Finally, new models of the expected SNR absorptions should be forthcoming based on the current knowledge about the character of the X-ray spectrum of SN 1006.

We thank our many colleagues on the HUT team and all of the NASA personnel who helped to make the Astro-2 mission a success. We also thank Francois Schweizer for digging into his archive to provide a tracing of the SM star spectrum, and Rex Saffer for consultation about subdwarf stars in general, PG 0839+399 in particular, and for attempting new fits to the SM star optical spectrum. Support for this work was provided by NASA contract NAS 5-27000 to the Johns Hopkins University and NASA grant NAG 8-1074 to the Smithsonian Astrophysical Observatory.

REFERENCES

Becker, R. H., Holt, S. S., Smith, B. W., White, N. E., Boldt, E. A., Mushotzky, R. F., & Serlemitsos, P. J. 1980a, ApJ, 235, L5
Becker, R. H., Szymkowiak, A. E., Boldt, E. A., Holt, S. S., & Serlemitsos, P. J. 1980b, ApJ, 240, L33
Becker, R. H., White, N. E., Boldt, E. A., Holt, S. S., & Serlemitsos, P. J. 1980c, ApJ, 237, L77
Bowers, C. W., Blair, W. P., Long, K. S., & Davidsen, A. F. 1995, ApJ, 444, 748
Cardelli, J. A., Clayton, G. C., & Mathis, J. S. 1989, ApJ, 345, 245
Davidsen, A. F., et al. 1992, ApJ, 392, 264
Dwek, E., Petre, R., Szymkowiak, A., & Rice, W. L. 1987, ApJ, 320, L27

Ekberg, J. O. 1993, A&AS, 101, 1
Fawcett, B. C. 1989, At. Data Nucl. Tables, 41, 181
Fesen, R. A., Wu, C. C., Leventhal, M., & Hamilton, A. J. S. 1988, ApJ, 327, 178
Garcia-Senz, D., & Woosley, S. E. 1995, ApJ, 454, 895
Green, D. A. 1995, A Catalogue of Galactic Supernova Remnants (1995 July version; Cambridge: Mullard Radio Astronomy Observatory) (URL: http://www.phy.cam.ac.uk/www/research/ra/SNRs/snrs.intro.html)
Green, R. F. 1980, ApJ, 238, 685
Green, R. F., Schmidt, M., & Liebert, J. 1986, ApJS, 61, 305
Hamilton, A. J. S., & Fesen, R. A. 1988, ApJ, 327, 178 (HF88)
Hamilton, A. J. S., Sarazin, C. L., & Szymkowiak, A. E. 1986, ApJ, 300, 698
Hubeny, I., & Lanz, T. 1995, ApJ, 439, 875
Hubeny, I., Lanz, T., & Jeffery, C. S. 1994, Newsletter on Analysis of Astronomical Spectra (St. Andrews: St. Andrews Univ.), 20, 30
Kirshner, R. P., Winkler, P. F., & Chevalier, R. A. 1987, ApJ, 315, L135
Koyama, K., Petre, R., Gotthelf, E. V., Huang, U., Matsuura, M., Ozaki, M., & Holt, S. S. 1995, Nature, 378, 255
Kriss, G. A. 1994, in ASP Conf. Series 61, Astronomical Data Analysis Software and Systems III, ed. D. R. Crabtree, R. J. Hanisch, & J. Barnes (San Francisco: ASP), 437
Kruk, J. W., Durrance, S. T., Kriss, G. A., Davidsen, A. F., Blair, W. P., Espey, B. R., & Finley, D. S. 1995, ApJ, 454, L1
Laming, J. M., Raymond, J. C., McGlaughlin, B., & Blair, W. P. 1996, in preparation
Lanz, T., & Hubeny, I. 1995, ApJ, 439, 905
Leahy, D. A., Nousek, J., & Hamilton, A. J. S. 1991, ApJ, 374, 218
Long, K. S., Blair, W. P., & van den Bergh, S. 1988, ApJ, 333, 749
Minkowski, R. 1966, AJ, 71, 371
Morton, D. C. 1991, ApJS, 77, 119
Morton, D. C., York, D. G., & Jenkins, E. B. 1988, ApJS, 68, 449
Nahar, S. N. 1995, A&A, 293, 967
Nomoto, K., Thielemann, F.-K., & Yokoi, K. 1984, ApJ, 286, 644
Press, W. H., Flannery, B. P., Teukolsky, S. A., & Vetterling, W. T. 1986, Numerical Recipes (Cambridge: Cambridge Univ. Press), 535
Pye, J. P., Pounds, K. A., Rolf, D. P., Smith, A., Willingale, R., & Seward, F. D. 1981, MNRAS, 194, 569
Raymond, J. C., Blair, W. P., & Long, K. S. 1995, ApJ, 454, L31
Reynolds, S. P., & Gilmore, D. M. 1986, AJ, 92, 1138
Saffer, R. A., Bergeron, P., Koester, D., & Liebert, J. 1994, ApJ, 432, 351
Saffer, R. A., & Liebert, J. 1994, in Proc. 9th European Workshop on White Dwarfs, ed. D. Koester & K. Werner (Dordrecht: Kluwer), 221
Savedoff, M. P., & Van Horn, H. M. 1982, A&A, 107, L3
Schaefer, B. E. 1996, ApJ, 459, 438
Schweizer, F., & Lasker, B. M. 1978, ApJ, 226, 167
Schweizer, F., & Middleditch, J. 1980, ApJ, 241, 1039 (SM80)
Shull, J. M., Snow, T. P., & York, D. 1981, ApJ, 246, 549
Shull, J. M., van Steenberg, M., & Seab, C. G. 1983, ApJ, 271, 408
Simon, K. P., Hunger, K., & Kudritzki, R. P. 1981, A&A, 98, 211
Smith, R. C., Kirshner, R. P., Blair, W. P., & Winkler, P. F. 1991, ApJ, 375, 652
van den Bergh, S. 1976, ApJ, 208, L17
Verner, D. A., Barthel, P. D., & Tytler, D. 1994, A&AS, 108, 287
Wesemael, F., Fontaine, G., Bergeron, P., Lamontagne, R., & Green, R. F. 1992, AJ, 104, 203
Willingale, R., West, R. G., Pye, J. P., & Stewart, G. C. 1996, MNRAS, 278, 749
Winkler, P. F., & Long, K. S. 1996, in preparation
Woosley, S. E., & Weaver, T. A. 1987, in IAU Colloq. 89, Radiation Hydrodynamics in Stars and Compact Objects, ed. D. Mihalas & K.-H. A. Winkler (Berlin: Springer), 91
Wu, C. C., Crenshaw, D. M., Fesen, R. A., Hamilton, A. J. S., & Sarazin, C. L. 1993, ApJ, 416, 247